



Characterization of Martensite Orientation Relationships in Steels and Ferrous Alloys from EBSD Data Using Bayesian Inference

A.F. BRUST, E.J. PAYTON, V. SINHA, V.A. YARDLEY, and S.R. NIEZGODA

Detailed analysis of the characteristics a martensite structure inherits from the parent austenite phase requires knowledge of the crystallographic orientation relationship between austenite and martensite, which varies with composition for steel alloys. The orientation relationship is typically observed to exhibit a significant degree of variability, such that measurements from each variant occupy a range of orientations within the transformed pole figure, complicating characterization of the orientation relationship. Here, we present a Bayesian methodology to measure the orientation relationship on martensite EBSD data from four different steels and a binary Fe-Ni alloy. The number of variants that must be exhibited for an accurate measurement as well as robustness to noisy data for this approach are investigated. The Bayesian approach is found to produce results which compare favorably to those from prior work while being more easily automatable.

<https://doi.org/10.1007/s11661-019-05514-4>

© The Minerals, Metals & Materials Society and ASM International 2019

I. INTRODUCTION

IN steels with a carbon content of 0.6 pct or below, the austenite phase (γ) transforms athermally to the metastable martensite phase (α') when the cooling rate from the austenite phase field is sufficiently rapid. For many steel compositions, the transformation goes to completion such that only the martensite phase is observable at room temperature. With little to no remaining austenite, the morphology and orientation of the parent austenite grains can only be inferred from observations of martensite.

The transformed microstructure exhibits a hierarchical arrangement of up to 24 crystallographic variants of the original austenite grain orientations.^[1,2] Blocks are composed of pairings of the variant orientations that

nominally share the same austenite c-axis, and are grouped together into packets that nominally share a habit plane.^[1,3] Crystallography of the face-centered cubic transformations to body-centered cubic or body-centered tetragonal crystal structure dictates that there are four possible habit planes. While 24 variants are possible for each austenite orientation, not all must be exhibited within a grain and observation of the microstructure in cross-section results in the possibility that only a subset of the variants existing for a given grain is observed. A single prior austenite grain (PAG) grain can form up to four specific packets, each with a specific habit plane. Up to three blocks can be contained within a single packet, with each block consisting of a pair of crystallographically similar variant orientations separated by a low-angle misorientation.

The prior austenite grain structure is known to affect some properties, and therefore the performance in service of steel used in the quenched and tempered conditions. These include a ductile to brittle fracture transition,^[4,5] the identification of creep and cavitation sites,^[6,7] and temper embrittlement due to impurity segregation at PAG boundaries.^[8,9] Traditionally, the assumed orientation relationship (OR) has been ascribed to one of two commonly referenced orientation relationships. The observance of 24 crystallographic variants leads to the citation of the most popular orientation relationship in steels, the Kurdjumov–Sachs (KS) orientation relationship:^[10]

$$\{111\}_{\gamma} // (011)_{\alpha'}; \quad \langle\bar{1}01\rangle_{\gamma} // \langle\bar{1}\bar{1}1\rangle_{\alpha'} \quad [1]$$

A.F. BRUST is with the Department of Materials Science and Engineering, The Ohio State University, Columbus, OH 43210. E.J. PAYTON is with the Air Force Research Laboratory, Materials and Manufacturing Directorate, Dayton, OH 45433. V. SINHA is with the Air Force Research Laboratory, Materials and Manufacturing Directorate and also with UES, INC., Dayton, OH 45433. V.A. YARDLEY is with Impression Technologies, Ltd., Coventry CV5 9PT, UK. S.R. NIEZGODA is with the Department of Materials Science and Engineering, The Ohio State University and also with the Department of Mechanical and Aerospace Engineering, The Ohio State University, Columbus, OH 43210. Contact e-mail: niezgoda.6@osu.edu

Manuscript submitted April 14, 2019.

Article published online November 18, 2019

The Nishiyama–Wassermann (NW) orientation relationship is called upon when approximately 12 crystallographic variants are observed due to alignment of symmetry elements.^[11,12]

$$\{111\}_\gamma//(011)_\alpha; \quad \langle\bar{1}\bar{1}2\rangle_\gamma//\langle0\bar{1}1\rangle_\alpha \quad [2]$$

The plane and direction parallelism in these orientation relationships have long been known not to be followed closely in real alloys. Greninger and Troiano described an irrational orientation relationship that falls somewhere between the KS and NW ORs in 1949^[13] (from here on in the present work referred to as GT). The actual irrational orientation relationship varies with composition for a given alloy;^[14,15] however, challenges in characterizing the orientation relationship usually lead to the assumption of one of the above two relationships. While the variation in the orientation relationship with composition can theoretically be predicted with the phenomenological theory of martensitic transformations,^[16–23] the theory cannot account for the variability in the orientation relationship which is experimentally observed within a nominally uniform specimen. Deviations may arise from local fluctuations in composition, cooling rate, and the extent of plasticity.^[24–26] Therefore, steels of the same grade from different lots or subjected to differing thermomechanical processing routes could each exhibit a slightly different orientation relationship.

As reconstruction of austenitic microstructures from observations of martensite is desired for a number of applications, and reconstruction reliability is improved with a measurement of the orientation relationship, there is a general need for programs that can accurately, efficiently, and automatically measure the orientation relationships in steels. Especially desirable would be programs that are user-friendly, allowing those with limited computational experience to effectively run them whilst performing the measurement in a timely manner.

Most existing methods for characterizing the orientation relationship in steels are tedious and require significant crystallographic expertise.^[15,27] Some require the isolation of a PAG before the OR can be computed.^[14,28,29] This limits the definition of an “automated” approach since a considerable amount of time must first be spent partitioning the PAG. Furthermore, the segmentation is presumptive, based on assumed PAG boundaries, thereby potentially limiting the accuracy of the results or requiring a tedious examination of the martensite microstructure in order to capture a certain PAG boundary. Other techniques exist that do not require the isolation of a PAG, relying instead on misorientation information of neighboring martensitic points.^[30–32] However, these techniques are highly dependent upon user-input tolerances and selection of the most “popular” Euler angle variants. This in turn can limit the accuracy, efficiency, and reproducibility of the results.

The following paper introduces a rapid, effective, and automatable method for characterization of the orientation relationship in martensitic steels. The OR

measurements were performed using MATLAB (R2016a, Mathworks, Inc., Natick, MA USA) from EBSD data sets of transformed martensite with use of the MTEX crystallographic data analysis toolbox.^[33]

II. METHODOLOGY

It is well known that 24 crystallographic variants are observed for the martensitic transformation in steel, with the notable exception of the NW OR.^[2,3] The crystallographic rotations corresponding to the variants may be described through the use of Euler angles. However, the Euler angle description is verbose since a full description of the OR requires a set of 24 Euler angles which are not unique, but vary by reference frame and convention for the order of rotation operation. A more compact notation for describing the orientation relationship, known as ξ angles, has been proposed by Yardley and Payton.^[4,6,15,29] The three ξ angles, representing deviations of primary α' axes from the Bain correspondence matrix of the phenomenological theory, can fully describe the entire OR. The procedure used to represent the OR through use of said ξ angles is almost equivalent to the one described by Kurdjumov and Sachs.^[10]

A complete description of these angles can be found in Reference 29 and, as such, a brief description will be provided below. To characterize the orientation relationship using ξ angles, Yardley & Payton manually selected regions from a single prior austenite grain in their martensite EBSD data sets, avoiding twins; then rotated the data so that the PAG orientation was coincident with the sample reference frame. The angular deviation between the closest Bain correspondence matrix axes^[34] and the primary axis of the rotation matrix could then be measured, producing ξ_1 , ξ_2 and ξ_3 , which correspond to the smaller and larger deviations between the $\langle110\rangle$ -type Bain correspondence axis, and the deviation from the $\langle001\rangle$ -type Bain correspondence axis, respectively.

A. Bayesian Statistics

The computation of the experimental OR was achieved by framing the problem as Bayesian inference.^[35] Bayesian statistics will only be briefly reviewed here; the interested reader can find a more detailed treatment in the following References 36 and 37. The Bayesian casting of potential solutions in terms of possible states of truth is useful when analysis must be performed on noisy and uncertain data.^[38,39] The martensitic microstructure in steels can exhibit up to $m \times 24$ crystallographic variants for m prior austenite grains. Unique determination of the parent austenite orientation requires observing an appropriate combination of variants. In addition, transformation-induced plasticity, variation in the OR, and uncertainty in the measurement further obfuscate the parent austenite orientation.

The main focus of Bayesian inference lies in the prior probability of an event A , denoted $P(A)$, which is then

updated given an observation, \mathbf{B} . This results in the establishment of the posterior probability distribution, which can be denoted as $P(\mathbf{A}|\mathbf{B})$. The following expression is known as the Bayes theorem:

$$P(\mathbf{A}|\mathbf{B}) = \frac{P(\mathbf{B}|\mathbf{A})P(\mathbf{A})}{P(\mathbf{B})} \quad [3]$$

where $P(\mathbf{A})$ is the belief about what event \mathbf{A} should be *before* the actual observation and $P(\mathbf{B})$ is related to the evidence and is simply the probability of obtaining the observation, \mathbf{B} . Through a Bayesian lens, from the prior proposition, we are simply attempting to find the maximizer of the posterior given our observation. An optimization of the posterior distribution therefore refers to the maximum a posteriori probability, commonly referred to as the MAP estimate, where $P(B)$ represents a conditional constant in regards to the maximization of the posterior and can be promptly ignored:

$$\begin{aligned} \hat{\mathbf{A}}_{\text{MAP}} &= \max_A P(\mathbf{A}|\mathbf{B}) \\ &= \max_A \left(\frac{P(\mathbf{B}|\mathbf{A})P(\mathbf{A})}{P(\mathbf{B})} \right) \\ &= \max_A (P(\mathbf{B}|\mathbf{A})P(\mathbf{A})) \end{aligned} \quad [4]$$

B. Formulation of the Inference Problem

Similar to other approaches by Miyamoto *et al.* and Payton *et al.*,^[15,27] our approach does not require an exact segmentation of the PAG in order to capture an accurate OR. Rather, in order to perform the measurement, a small section or window is extracted from the transformed EBSD data set, containing a set of n martensite orientations, $G_m = [g_m^{(1)}, g_m^{(2)}, \dots, g_m^{(n)}]$. Ideally, this region corresponds to a section of martensite points that have all transformed from the same assumed PAG with respect to the sample-specific OR—albeit, as demonstrated below, this is not absolutely necessary. The size of the selected region does affect the quality of the OR measurement, although the technique is robust enough to where the region can extend across what amounts to a PAG boundary while producing an accurate measurement. This is due to the Bayesian implementation, which can designate the overflowing orientations as variable noise and consequently identify orientations associated with the respective PAG. Additionally, the region can be small enough to where only a few different martensite variants reside, although too small of a region within the grain will result in a poor measurement (examples of extracted windows are displayed later in Figure 3).

Before describing the actual OR estimation procedure, it is instructive to consider a schematic picture model of how the measured martensite orientations, G_m , were produced from a prior austenite grain. Consider g_a to be the orientation of the idealized prior austenite grain. What's meant by idealized orientation is an assumption that the grain is a perfect single crystal with

no orientation gradients, misindexed points, *etc.* The transformation to martensite can then be represented by transforming g_a as $\Delta g_{\gamma \rightarrow \alpha}(\Xi^{(i)}) \equiv \Delta g_{\gamma \rightarrow \alpha}(\xi_1, \xi_2, \xi_3, v_i)$, which consequently produces an ideal martensite orientation. The OR is then represented as $\Xi^{(i)} = (\xi_1, \xi_2, \xi_3)$, and v_i indicates the transformation variant associated with an observed martensite point, $g_m^{(i)}$. Note that $\Delta g_{\gamma \rightarrow \alpha}(\Xi^{(i)})$ is a random variable as there are 24 possible martensite variants for the OR. For simplicity, we can ignore variant selection and assume that for each variant, the probability is 1 / 24 and the probability of a $\Delta g_{\gamma \rightarrow \alpha}(\Xi^{(i)})$ that doesn't correspond to an exact variant of the OR is zero. This idealized picture is overly simplistic, so an additional rotation is incorporated that accounts for noise or uncertainty, $\Delta g_{\gamma \rightarrow \alpha}^{(i)}(\kappa)$. This noise accounts for any source of deviation of the martensite orientation from the ideal transformation orientation and can in principle include: *i*) variability in the OR due to compositional effects or lattice parameter variations, *ii*) plastic deformation during the martensite transformation, *iii*) variability in the prior austenite grain orientation, *iv*) misindexed points or other sources of noise in the EBSD measurement, and *v*) points within the window excluding those from either a different prior austenite grain or prior austenite annealing twin. The noise is also a random misorientation assumed to be sampled from a unimodal misorientation distribution function, with halfwidth, κ , centered on the identity misorientation. The austenite to martensite transformation can now be modeled as:

$$g_m^{(i)} = \Delta g_{\gamma \rightarrow \alpha}^{(i)}(\kappa) \Delta g_{\gamma \rightarrow \alpha}(\Xi^{(i)}) g_a \quad [5]$$

Our objective is to infer the OR given the observed martensite orientations, G_m . In Bayesian terms, this inference can be cast as:

$$\pi(\Xi, \kappa | G_m) \propto \prod_{i=1}^N f(g_m^{(i)} | g_a, \Xi, \kappa) f(g_a | \Xi, \kappa) \pi(\Xi) \pi(\kappa) \quad [6]$$

where $\pi(\Xi, \kappa | G_m)$ is the posterior probability distribution of the orientation relationship and noise level given the observed martensite orientations. Additionally, the likelihood of observing the measured martensite orientations given values of the prior austenite orientation, OR, and noise is $f(G_m | g_a, \Xi, \kappa) = \prod_{i=1}^N f(g_m^{(i)} | g_a, \Xi, \kappa)$. Note that the prior austenite orientation is an unknown and can be considered a hidden variable in the model, and $f(g_a | \Xi, \kappa)$ is a likelihood of the prior austenite orientation given the OR and noise. The product, $f(G_m | g_a, \Xi, \kappa) f(g_a | \Xi, \kappa)$, is the overall data likelihood and can then be interpreted as the overall probability of observing the martensite orientations given both the OR and noise. Finally, the prior probability distributions on the OR and noise are $\pi(\Xi)$ and $\pi(\kappa)$, respectively.

The data likelihood function is constructed by considering the schematic model of the martensite transformation described above. With this consideration, the prior austenite grain can be transformed by the OR to generate orientations related to all 24 potential

martensite variants. These variants are then convolved with the noise kernel (unimodal ODF with halfwidth κ) to produce an ODF. When this ODF is evaluated for any martensite orientation, it returns the probability that the martensite orientation was generated by the transformation of the prior austenite orientation given the OR and noise. Therefore, this ODF serves as our desired likelihood function, $f(g_m|g_a, \Xi, \kappa)^*$.

*Strictly speaking, this results in an ODF that is proportional to, but identically equal to, the ODF. The ODF is not formally a probability distribution as it is scaled by multiples of the uniform random distribution, making it easy to interpret relative probability in terms of “times random.” This results in a proportionality factor equal to the volume of the fundamental zone for cubic orientations. However, this can be neglected as it is a constant term which can be divided out and incorporated into the proportionality factor in Eq. [6].

The likelihood function for the prior austenite orientation, $f(g_a|\Xi, \kappa)$, is also an ODF but unfortunately does not appear to have a simple form and thus must be approximated. This approximate likelihood can be constructed by the following process: 1) Compute the inverse of the transformation Ξ to get the set of martensite \rightarrow austenite OR. 2) Apply the inverse transformation to all martensite orientations in G_m . This will result in 24 potential austenite orientations for each observed orientation. 3) Compile the complete set of potential austenite orientations over all observed martensite orientations and calculate an ODF by kernel density estimation using a narrow smoothing kernel. An ODF constructed in this manner turns out to be an excellent approximation for the probability distribution for a prior austenite orientation. Ultimately, the construction of the ODF can be likened to a voting process. Each observed martensite “votes” for 24 potential austenite orientations (given the OR). Since all of the martensite orientations ideally come from the same prior austenite grain, all of the “votes” for the actual austenite orientation will be clustered and the other 23 will be spread nearly uniformly over the orientation space. Kernel density estimation produces an ODF with one very dominant mode that is sharply peaked. In practice, the estimation is not very sensitive to the halfwidth of the kernel used for ODF construction, provided it is not too broad, as it has the same effect on all of the “votes.” The modal orientation of the ODF is remarkably insensitive to the kernel halfwidth. A value of 0.25κ or even smaller was found to be sufficient for the ODF estimation. In testing with virtual data sets, where the prior austenite orientation was known *a priori*, it was found that, provided a reasonable window was selected to create G_m , the modal orientation was virtually always within $\leq \pm 1$ deg (or approximately to within the accuracy of EBSD measurement) to the ground-truth prior austenite orientation. This allows us to simplify the calculation of the posterior by only considering the modal prior austenite orientation, g_a^{modal} :

$$\pi(\Xi, \kappa|G_m) \propto \prod_{i=1}^N f(g_m^{(i)}|g_a^{modal}, \Xi, \kappa) f(g_a^{modal}|\Xi, \kappa) \pi(\Xi) \pi(\kappa) \quad [7]$$

This effectively transforms the unknown hidden variable into a known quantity, thereby reducing the dimensionality of the search space and simplifying the inference problem.

Payton and Yardley^[4] previously observed that the measured values for the angles (ξ_1, ξ_2, ξ_3) fit well to a folded or wrapped normal distribution, which takes the form:

$$p(x) = \frac{1}{\sigma\sqrt{2\pi}} e^{-\frac{(x-\mu)^2}{2\sigma^2}} + \frac{1}{\sigma\sqrt{2\pi}} e^{-\frac{(x+\mu)^2}{2\sigma^2}} \quad [8]$$

For this work, we adopt this observation to form the prior probability, $\pi(\Xi) = \pi(\xi_1)\pi(\xi_2)\pi(\xi_3)$, where each ξ_k value is assumed to be *a priori* independent and $\pi(\xi_k)$ is represented by a wrapped normal. The means were set to $\mu_{\xi_1} = 5$ deg, $\mu_{\xi_2} = 9$ deg, $\mu_{\xi_3} = 10$ deg, which is approximately in-between the GT and KS ORs, and the standard deviations were set to $\sigma = 1.2$ deg. This was found to work well for the full range of ORs from NW to KS. It is expected that, provided the window is reasonably selected, the noise kernel should be relatively small; therefore, the prior monotonically decreases and approaches zero at large noise values. For simplicity, we also chose a wrapped normal for $\pi(\kappa)$ with $\mu_\kappa = 1$ deg and a standard deviation of 2 deg. This approximates a uniform probability over the range from [0, 1] rather than a fairly rapid decay.

C. MAP Estimate and Posterior Distribution

A Maximum A Posteriori (MAP) estimate of the OR and noise halfwidth was achieved by way of maximization of the aforementioned likelihoods in Eq. [7]. The optimization was achieved with a built-in MATLAB function, “fminunc”, which applies an unconstrained gradient search approach. An initial guess for both the OR (Ξ^i) and the halfwidth (κ^i) were provided, where Ξ^i was chosen to be the KS OR and κ^i was arbitrarily chosen to be 3 deg. Although the initial choice for the OR is chosen as KS as an “outer-bound” of a physically relevant OR, the technique is robust enough to handle a wide range of values. For instance, the KS, NW, and a randomly chosen OR outside the range of the two cited ORs produced consistent results for the same respective sample.

The MAP estimate provides us with our best guess of the average OR relationship given the observed martensite orientations. However, for this work, we are also interested in quantifying the uncertainty in the OR measurement. We adopt a Markov Chain Monte Carlo (MCMC) method to generate samples from the posterior distribution of the OR. MCMC combines two differing properties: *Monte Carlo* and *Markov Chain*.

The former refers to an estimation of the properties of a particular distribution through an examination of random samples from the distribution. *Markov Chain* is then related to the notion that a sequential process generates the random samples. In other words, a sample obtained from a previous iteration is consequently used to generate the next random sample, and so on.

We apply the standard Metropolis Hasting algorithm^[40,41] to generate samples from the posterior distribution. For the interested reader, refer to additional standard texts for a complete description of the method.^[42,43] Conceptually, the algorithm is quite straightforward, beginning with the generation of a sequence of samples from the posterior distribution using the Metropolis Hasting algorithm. At each iteration, the algorithm picks a candidate OR through a slight perturbation of the current value. If this candidate has a higher likelihood than the current OR, it is accepted. If it has a lower likelihood, it is either accepted with a probability based on the ratio detailing the likelihood of the candidate OR with the likelihood for the current OR. In other words, the probability of acceptance is dependent upon how much worse the candidate is vs. the current value. Therefore, if the proposed likelihood is 50 pct worse than the current likelihood, the probability of acceptance would be 0.5.

In our case, we chose to sample the ξ angles individually rather than in a block. We found that the OR and corresponding noise parameters were converged after approximately 2e4 iterations, with 0.1 deg variation in the mean value of the ξ angles reached in less than 20 minutes on a 3.4 GHz single core processor. From the generated distributions, the resultant mean of the individual ξ_k angles is taken as the output OR, which comes with a corresponding likelihood value that can effectively detail the accuracy of the computation. Additionally, a random set of orientations computed from the designated OR corresponding to the transformation $g_a \rightarrow G_m^a$ can be plotted as a pole figure and compared with the input martensite orientations from the PAG to ensure an appropriate OR was constructed.

III. RESULTS

A selection of different martensitic steel and binary alloy data sets were studied to highlight the deviation from ideal ORs that has been analyzed previously in the literature. These samples were chosen because they were expected to exhibit disparate ORs (KS-like, GT-like, and NW-like) due to the variability in their respective compositions, which in turn would illustrate the robustness and range of applicability of the method.^[13,15,28,29,44] Additionally, the effects of the number of data points from a single PAG and the effects of inclusion of points from different PAGs were analyzed using different window sizes with a window centered over a single PAG in a data set. Finally, a large data set was chosen where regions from several different grains were selected in order to test the precision of the code for repeat measurements on materials of the same composition and processing history.

A. Variation of OR with Composition

The ORs for three samples with distinctly different compositions were determined and compared with experimental validation pulled from results by Payton and Yardley.^[29] The two steel samples were a low-carbon steel, whose composition can be found in^[45] and would suggest a KS-like OR; FV535 steel (German grade X8CrCoNiMo11), a tempered martensitic, heat-resistant steel that should fall in-between KS and NW, and thus exhibits a ‘GT-like’ OR; and the binary ferrous alloy was an Fe-30 at. pct Ni alloy that should have a NW-like OR.^[2,24] For experimental details, including specimen processing methodology and data aquisition information, the reader is referred to Reference 29.

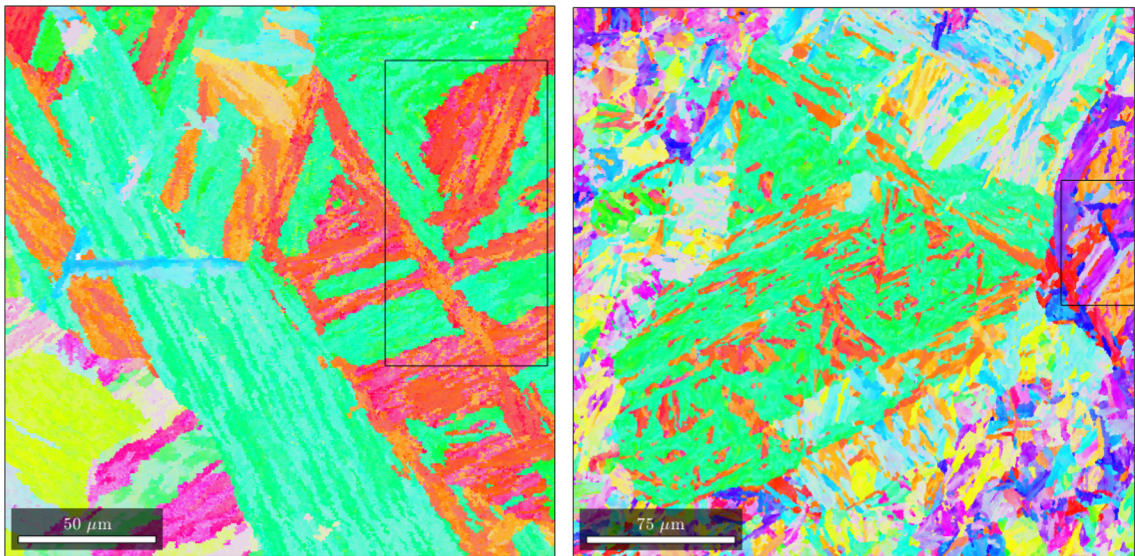
The Low-C and the FV535 $\gamma \rightarrow \alpha'$ transformations go to full completion, while the Fe-30Ni sample has a substantial amount of retained austenite (~ 15 pct), which shows up as the black spaces in Figure 1(c). Austenite data points were excluded from the analysis and the inverse pole figure (IPF) maps for the sample surface normal direction (Z) for the martensite phase are given in Figure 1 for each steel. The window boundaries shown in black correspond to the analyzed regions containing only data from a single PAG.

Visual inspection of the IPF maps for each steel reveals substantial variation in the transformed martensite microstructure. The low-C sample (Figure 1(a)) exhibits lath-like crystallite morphology whereas the Fe-30Ni sample (1c) exhibits a more plate-like morphology, with retained austenite sprinkled throughout the microstructure. The scale of the microstructure is different for each material, with the largest block and packet size being observed in the low-carbon steel.

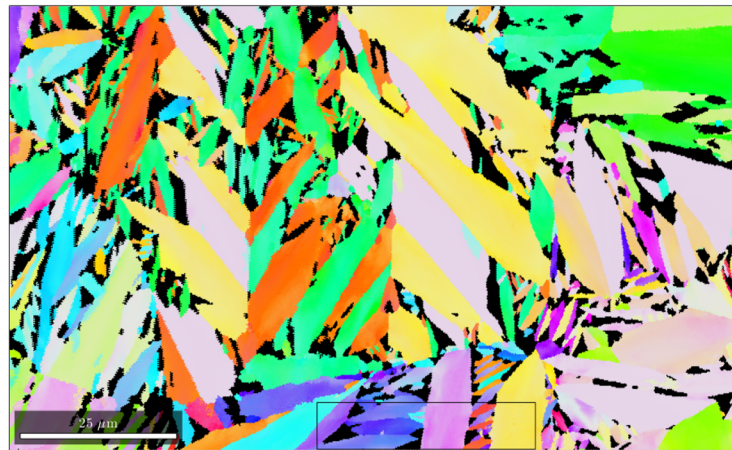
The previously measured ORs for each specimen are given in Table I along with the Bayesian OR estimate, the expected approximate theoretical OR (KS, NW, or GT), the noise, and the variance associated with each respective ξ value, σ^2 . It should be noted that for GT, there are a range of ORs which can satisfy multiple ORs. To obtain the GT OR used in the present work, the mean ξ parameters were obtained from a simulated data set consisting of 5e5 random orientations that met the criteria described by Greninger and Troiano:^[13]

- (1) 1 deg deviation of $\{111\}_\gamma$ from $\{011\}_\alpha'$
- (2) 2.5 deg deviation of $\langle\bar{1}01\rangle_\gamma$ from $\langle\bar{1}\bar{1}1\rangle_\alpha'$
- (3) 2.0 deg deviation of $\langle\bar{1}\bar{1}2\rangle_\gamma$ from $\langle0\bar{1}1\rangle_\alpha'$
- (4) 6.5 deg deviation of $\langle0\bar{1}1\rangle_\gamma$ from $\langle\bar{1}\bar{1}1\rangle_\alpha'$

The results of the Bayesian OR estimation show good agreement with the previous experimental measurements from Yardley and Payton.^[29] The measured ORs for each of the samples are clearly distinguishable from one another, highlighting the robustness of ξ parameter approach to characterizing the OR. The discrepancy between the commonly-cited theoretical ORs and their respective experimentally-observed counterparts, especially low-C with KS, underscores that the



(a) IPF map for the transformation product of a low-carbon steel (b) IPF map for the transformation product of the FV535 steel sample



(c) IPF map for the transformation product of the Fe-30Ni steel specimen

Fig. 1—IPF maps for the low-C (top left), FV535 (top right), and Fe-30Ni (bottom) samples, with overlaying IPF key.

measured ORs differ substantially from the theoretical ORs that are typically cited in the literature for these compositions. This topic will be detailed further in the Discussion section.

Since many readers may not be familiar with the ξ angle OR characterization technique, $\{001\}_{\omega}$ pole figures have also been plotted in Figure 2 and the Bunge Euler angles for a representative variant of each Bayesian estimate for the OR were computed. The pole figures in the center column of Figure 2 are a sample of 2000 martensite orientations from within the boxed regions in Figure 1. The “computed” pole figures show 2000 martensite orientations obtained by sampling our distribution centered by the prospective austenite orientation, g_a , which in turn is transformed into a set of randomly generated martensite orientations based on the ξ values and relative noise, κ , associated with the input data set. The computed austenite orientations are listed here in terms of Euler angles (ϕ_1, Φ, ϕ_2): for the

Fe-30Ni sample, $g_a = [111.78 \text{ deg}, 40.77 \text{ deg}, 286.05 \text{ deg}]$; $g_a = [4.26 \text{ deg}, 42.97 \text{ deg}, 4.55 \text{ deg}]$ for the FV535 sample; and for the low-C sample, $g_a = [339.63 \text{ deg}, 0.29 \text{ deg}, 19.54 \text{ deg}]$. Additionally, the computationally determined halfwidths (κ) and variance of the ξ angles (σ^2) after 2e4 iterations are also listed in Table I.

Finally, for comparison, the $\{001\}_{\gamma}$ pole figures for martensite orientations generated from the computed ORs, the EBSD-indexed martensite orientations, and their respective, commonly-cited theoretical counterparts are plotted in Figure 2. The commonly-cited ORs (KS, GT, and NW) have two different pole figures. The red points represent single variant orientations without the inclusion of any scatter or noise, and the blue points are a set of 2000 martensite orientations generated using the same halfwidth parameter as the computational cases for low-C, FV535, and Fe-30Ni, but use the theoretical OR instead of the Bayesian estimate as the mean variant locations. This creates an image that

Table I. Bayesian Measurement of ORs and Corresponding Halfwidth and OR Distribution Variance for the Three Samples Compared with Prior Experimental Measurements^[29] (Indicated by “P–Y”) and the KS, GT, and NW Theoretical ORs

Steel Sample	ξ_1 (deg)	ξ_2 (deg)	ξ_3 (deg)	κ	$\sigma^2(*1e^{-3})$
NW	0.0	9.74	9.74		
Fe-30Ni P–Y	1.87	9.16	9.18		
Fe-30Ni	1.63	9.19	9.19	1.10	[8.1, 2.2, 1.9]
GT	2.16	8.06	8.30		
FV535 P–Y	2.73	9.01	9.20		
FV535	2.42	9.09	9.24	1.42	[7.4, 3.5, 4.4]
KS	5.26	10.30	10.53		
Low-C P–Y	3.38	8.31	8.60		
Low-C	3.17	8.27	8.62	1.61	[17.4, 4.9, 8.5]

allows for a visual analysis of the accuracy of the computed ORs by comparison to the experimental martensitic data.

Note that the experimental and computed martensite orientations are almost exactly aligned for each case, barring variant selection and/or incomplete martensitic orientation data. The similarities between the experimental and computed pole figures for each specific sample coupled with the proximity of the numeric ξ angles in Table I suggests high accuracy of the Bayesian technique. The KS case is observed to differ significantly from the low-C steel experimental observation and computed OR, while a significantly smaller discrepancy between the theoretical OR and either the experimental observation or the Bayesian estimate is observed in the case of NW/Fe-30Ni or GT/FV535.

B. Effect of Varying Window Size During OR Estimation

To assess the robustness of our algorithm, the OR was measured for a series of six window sizes, capturing the effects on the number of observed variants, number of included data points, and data points corresponding to orientations from different prior austenite grains. The first four windows (A–D in Figure 3) contain only data from a single prior austenite grain, while windows E and F contain data points from multiple adjacent PAGs. For this analysis, a fourth steel specimen was used: an ASTM P122 12 wt pct Cr steel, for which processing and data collection conditions have also been described elsewhere, in References 4 and 6. Again, results are compared with a prior experimental determination of its OR.^[4]

If too few variants are observed, a unique prior austenite orientation cannot be determined. If a sufficient number of variants is observed for a unique PAG orientation determination but too few data points are included for each of those variants, then the scatter in the orientation relationship will not be well-characterized. If data points from multiple PAGs are included for fitting the OR and PAG orientation, the accuracy of proposed austenite orientations and corresponding likelihoods becomes diminished, resulting in poor choices of Ξ .

For the EBSD data shown in Figure 3, the presumed PAG is centrally located in the IPF-Z map. For validation, the authors performed a single grain

austenite reconstruction on this same data set in Reference 46, verifying the identity of the PAG. The computed ORs from the G_m array extracted from each window are given below in Table II, which also includes the number of data points within each window and the experimentally determined OR for validation.

For each respective case, the number of randomly chosen martensite orientations for G_m was 2000 from within the window size except for Windows A and B, which had only a maximum of 328 and 885 indexed data points. With only the slight increase in window size from A to B, however, a sufficient number of additional variants is observed for accurate characterization of the OR. Note that most of the possible variants are still not observed within Window B. This again suggests a robustness to the code that allows it to handle not only a wide range of different martensitic steel data sets but also regions within PAGs that may not fully represent the $\gamma \rightarrow \alpha$ transformation. As Table II suggests, Windows B through E produce accurate results, with Window D producing almost exactly the same OR as the one from Payton and Yardley.^[29]

Window A contains too few variants and Window B, with only the addition of a few more, regains traction and is reasonably accurate. Conversely, we can see that while Window E extends across the PAG boundaries, the fraction of data points from other PAGs is small enough that an accurate OR can still be reasonably characterized. Window F stretches too far outside of the PAG boundary, resulting in too much noise and thus a poor characterization of the OR. The pole figures for these four cases are shown in Figure 4 and exhibit the effect of window size on variant accessibility, where the addition of only a few more variants in Window B separates it from Window A. Additionally, it also displays how the algorithm can handle some noise present in Window E but, if the fraction of spurious points becomes too large, such as in Window F, it becomes too hard to sift through the noise to capture variants consistent to the prior austenite orientation.

It is clear that Window E contains a substantial amount of noise from orientations extending outside of the desired PAG and/or poorly-indexed orientations, but the determined OR retains accuracy. The pole figure corresponding to Window B lacks the characteristic symmetry common for martensite pole figures from

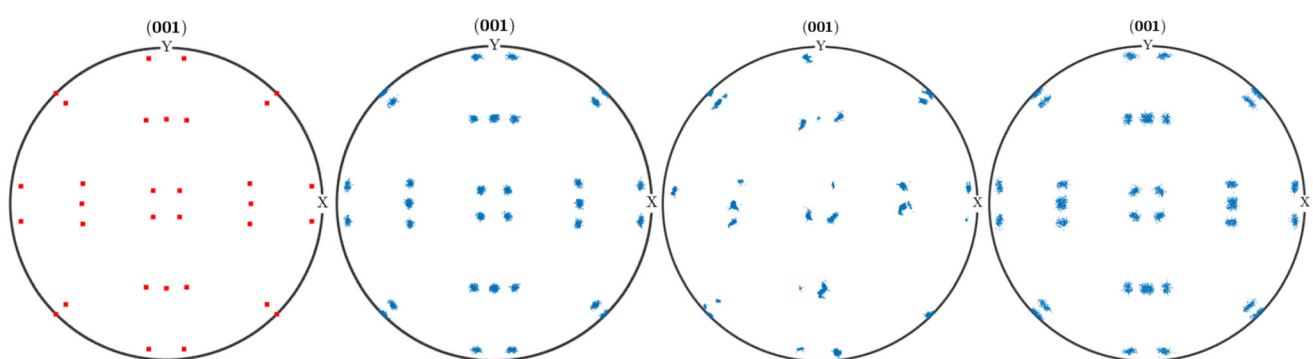
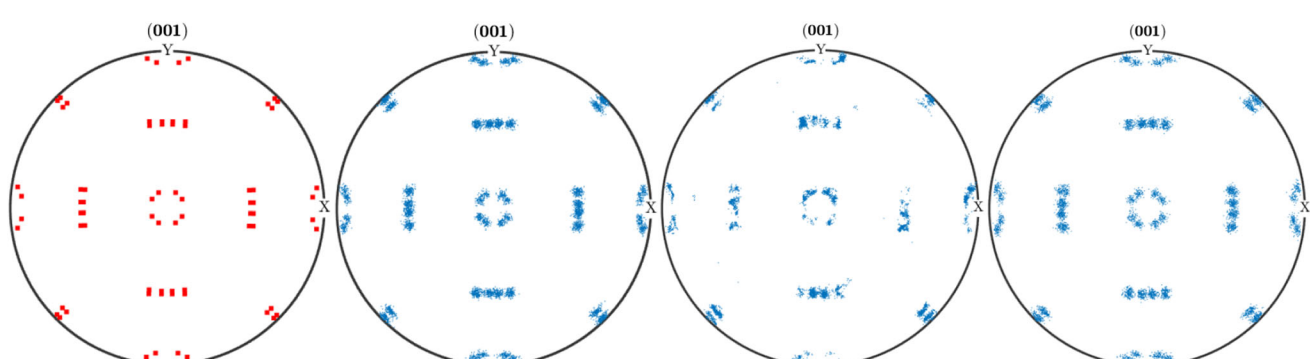
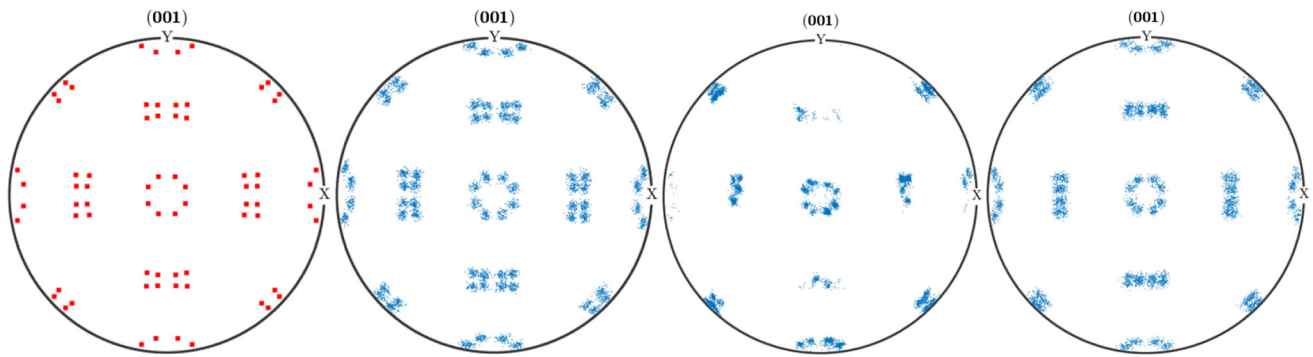


Fig. 2—The set of variants for the theoretical ORs of KS, GT, and NW (far left column), martensite orientations rotated by the inverse of their respective austenite orientations and displayed on {001} pole figures for KS, GT, and NW (middle left column), the experimental martensite data for the low-C, FV535, and Fe-30Ni samples (middle right column) and the martensite points generated from the Ξ, κ parameters from the input experimental data (far right column).

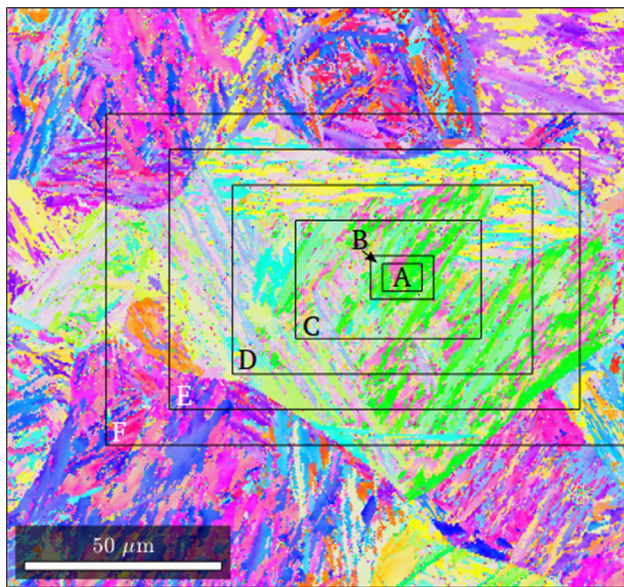


Fig. 3—IPF map of P122 martensitic steel containing variable window sizes of martensitic variants.

Table II. Computationally Determined ξ Angles for Variable Window Sizes of the P122 Steel Sample, Including Number of Data Points for Each Window and the Payton–Yardley (P–Y) Determined OR

Figure Label	ξ_1	ξ_2	ξ_3	Number of Data Points
Window A	2.31	10.35	10.28	328 pts
Window B	2.56	9.19	9.39	812 pts
Window C	2.59	8.87	9.11	6521 pts
Window D	2.61	8.99	9.21	16927 pts
Window E	2.57	8.88	9.10	31901 pts
Window F	9.87	14.55	14.20	51119 pts
P–Y	2.62	8.98	9.21	

single PAGs (Bain circles, *etc.*); however, the code is still able to converge upon a reasonable guess for the OR from the few present variants. The polar cases of Window A and Window F contain too few variants or too much noise to produce an accurate guess as to the PAG orientation.

IV. CORRELATION OF ξ ANGLES

The MAP-estimated ξ angles exhibit some correlation trends which were examined using matrix-based scatter plots, shown in Figure 5 for the low-C sample examined in the present work. The diagonal components display the posterior distributions of the individual ξ angles as histograms, where $2e4$ sets of ξ angles were computed. It should be noted that these distribution should be interpreted as a measure of the uncertainty in the measurement of the average OR. They are not representative of the spatial variability of the OR within a sample which will have a significantly larger variance than our estimate of the average or effective OR. The offset regions detail scatter plots of ξ_i vs. ξ_j , where the relative correlation can be visually assessed.

We can see that ξ_1 shows no correlation to either ξ_2 or ξ_3 , as the distribution is a randomly dispersed cloud. However, ξ_2 and ξ_3 show a strong, linear correlation to each other. This hints at the possibility of characterizing the OR through only a pair of angles with the inclusion of ξ_1 if a full measurement be unavailable, and then extrapolating to find the value of whichever angle of ξ_2 or ξ_3 was not used.

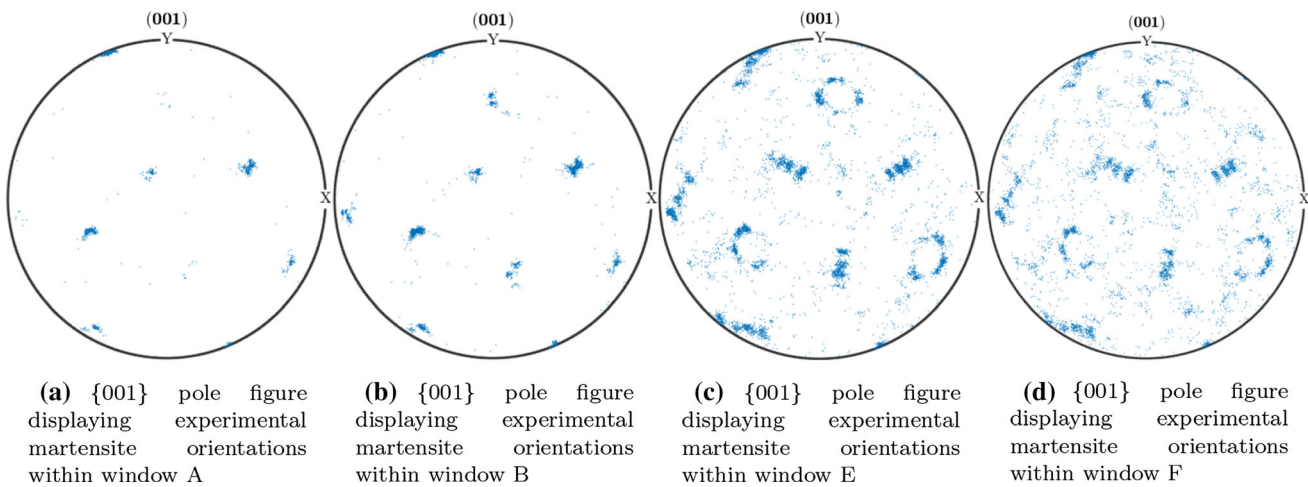


Fig. 4—{001} martensitic pole figures on ASTM P122 12 wt pct Cr steel sample for a selection of four variable windows.

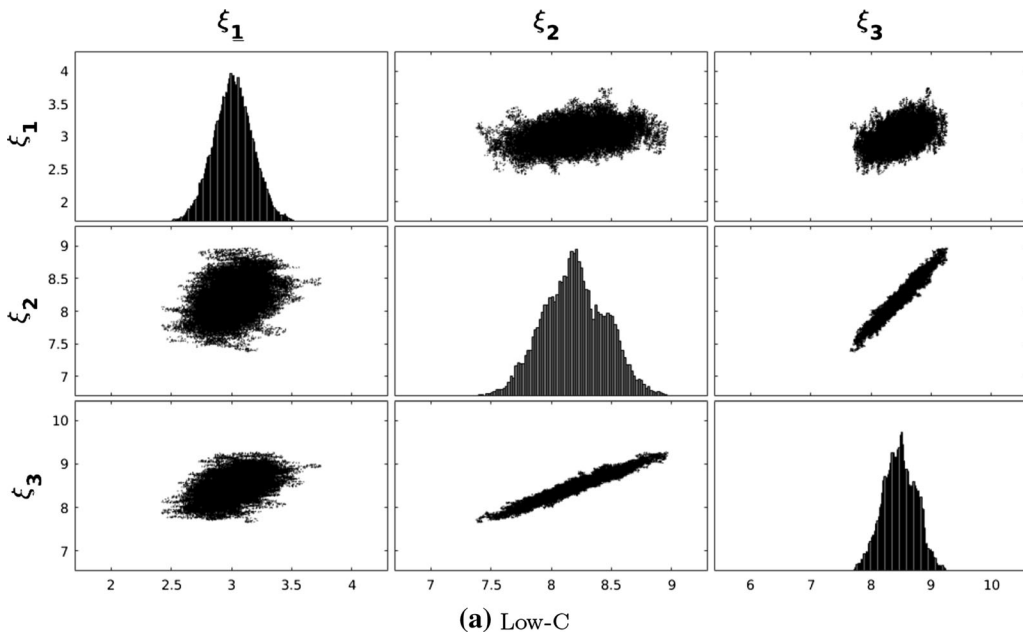


Fig. 5—Correlation plots and histogram distributions of computed ξ angles for the low-C steel specimen.

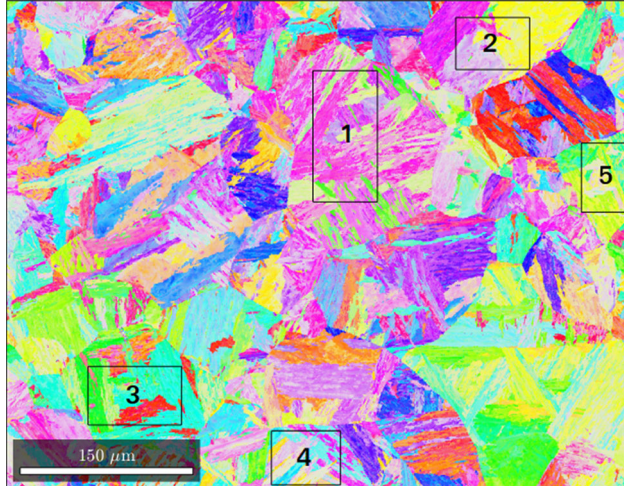


Fig. 6—Five labeled regions within five independent grains for the same AF9628 steel sample.

A. Reproducibility of OR Measurement

To assess the repeatability of OR measurements within a single specimen, we computed the OR for several different PAGs within a large area EBSD scan from a low-alloy, high-performance steel, AF9628.^[47] Processing parameters for this specimen have been published elsewhere, in Reference 48. The regions from single PAGs selected for analysis can be seen below in the IPF-Z map in Figure 6. Measurement results are given in Table III.

As can be seen in Table III, the Bayesian estimate results are very consistent and repeatable across several grains within the same data set. Although the PAGs themselves vary in both size of and number of

transformed martensite variants, the ξ values obtained for each grain are consistent to two significant figures.

V. DISCUSSION

Employing a Bayesian approach explicitly acknowledges the probabilistic nature of the OR estimate given the convolution of the observed scatter in the OR with measurement uncertainty. Section 3.1 examined characterization of the OR on three steels with different compositions. The three compositions were selected to illustrate the breadth of applicability of this approach to different compositions and the robustness to transformation product morphology and crystallography. Low-C steels exhibit a lath-like morphology with a crystal structure exhibiting little, to any, tetragonality depending on the carbon content and are typically assumed to exhibit a KS-like OR.^[2,49] The hierarchical arrangement of 24 variants can produce 16 boundary misorientations within a single PAG,^[44] and these boundaries serve as hindrances to plastic deformation affecting the toughness of the transformed steels.^[50–53] Steels with a Ni content above 28 pct exhibit NW-like ORs,^[24,49,54] for which it is often assumed there are only 12 variants corresponding to five unique boundary misorientations.^[44] The variations between the actual, irrational ORs and the idealized versions commonly cited are also evident when the {001} pole figures in Figure 2 are analyzed. For instance, the circular arrangement of PAG-transformed martensite orientations in the center of the pole figures is much larger in the KS case as opposed to the experimental/computational low-C case. Additionally, if we consider the streaks of orientations similar to lines surrounding the circular region, we can see variable numbers of “clusters” of points. With KS, eight distinct clusters are

Table III. Computed ORs from Five Different Grains Within the Same AF9628 Steel Specimen, with Numbering Corresponding to Fig. 6

Grain	ξ_1	ξ_2	ξ_3	Likelihood	Data Points in Windows
Grain 1	3.09	8.10	8.48	550.4	25877
Grain 2	3.07	8.12	8.57	513.7	11739
Grain 3	3.09	8.15	8.56	530.9	16789
Grain 4	3.02	8.11	8.53	547.3	11495
Grain 5	3.04	8.15	8.57	511.6	9638

visible, but the corresponding lines with the actual low-C sample show only four distinct clusters. The Fe-30Ni and NW case show a similar arrangement of orientations, although the former case displays clusters with broader ranges and thus encompasses more of the orientation spectrum. Furthermore, the pole figures here include noise, which further broadens the range of martensite locations and provides better agreement with experimental observation than the KS or NW OR descriptions, which do not account for any irrational variation between the parallel planes and directions.

The Bayesian approach exhibited robustness to a relatively small number of observed variants as well as to the incidental inclusion of orientations not belonging to the prior austenite grain of interest (Figures 3 and 4). We found the results from the approach to have excellent duplicability within different grains in a specimen (Figure 6 and Table III). Furthermore, all results agreed well with prior work. Accurate and repeatable measurement of the OR is a necessary prerequisite for reconstruction of the prior austenite microstructure from the observable martensitic data. For the Fe-30 at. pct Ni sample, the austenite orientation predicted from our OR measurement is misoriented from the mean of the retained austenite orientation by 1 deg, which is on the order of the accuracy expected of Hough-transform indexed EBSD patterns. Miyamoto *et al.*^[14] have shown that implementing an incorrect OR on austenite reconstructions leads to errors in both predictive PAG boundaries and orientations.

VI. CONCLUSION

The analysis of the four steel and ferrous binary alloy samples was performed to determine the accuracy and efficacy of the proposed Bayesian austenite to martensite orientation relationship measurement technique in steels and ferrous alloys. The proposed technique and methodology can be used to compute accurate OR measurements for the $\gamma \rightarrow \alpha'$ transformation across a broad range of steel compositions and martensite morphologies, is repeatable, and is reasonably robust so long as a sufficient number of variants is observed and a reasonable fraction of the EBSD data points originate within a single PAG.

ACKNOWLEDGMENTS

AFB and SRN received support from the Air Force Office of Scientific Research (AFOSR) Summer Faculty Fellowship Program (SFFP) for the portion of this work performed at the Materials and Manufacturing Directorate of the Air Force Research Laboratory (AFRL/RX) and from the Defense Associated Graduate Student Innovators (DAGSI) for the portion of the work performed at The Ohio State University.

REFERENCES

1. S. Morito, Y. Adachi, and T. Ohba: *Mater. Trans.*, 2009, vol. 50, pp. 1919–23.
2. H. Kitahara, R. Ueji, N. Tsuji, and Y. Minamino: *Acta Mater.*, 2006, vol. 54, pp. 1279–88.
3. S. Morito, H. Tanaka, R. Konishi, and T. Maki: *Acta Mater.*, 2003, vol. 51, pp. 1789–99.
4. V.A. Yardley, E.J. Payton, T. Matsuzaki, R. Sugiura, A.T. Yokobori Jr., S. Tsurekawa and Y. Hasegawa: Creep and Fracture of Engineering Materials and Structures, Proc. 12th Int. Conf. Creep and Fracture of Eng. Mater. and Struct. (JIMIS 11), held at Kyoto TERRSA, Kyoto, Japan, May 27–31, 2012, Edited by: K. Maruyama, F. Abe, M. Igarashi, K. Kishida, M. Suzuki, K. Yoshimi, The Jap. Ins. of Met, Sendai, 2012, paper C14.
5. K. Kimura, N. Ohi, K. Shimazu, and T. Matsuo: *Scripta Mater.*, 1987, vol. 21, pp. 19–22.
6. V.A. Yardley, S. Fahimi, and E.J. Payton: *Mater. Sci. Technol.*, 2015, vol. 31, pp. 547–53.
7. S.H. Hong and J. Yu: *Scripta Mater.*, 1989, vol. 23, pp. 1057–62.
8. S.K. Banerji, C.J. McMahon, Jr., and H.C. Feng: *Metall. Trans. A*, 1978, vol. 9A, pp. 237–47.
9. R.M. Horn and R.O. Ritchie: *Metall. Trans. A*, 1978, vol. 9A, pp. 1039–53.
10. G. Kurdjumow and G. Sachs: Über der Mechanismus der Stahlhärtung (On the Mechanism of Hardening of Steel) *Z. Phys.*, 1930, vol. 64, pp. 325–43.
11. Z. Nishiyama: X-ray Investigation of the mechanism of the transformation from face-centered cubic to body-centered cubic *Sci. Rep.*, 1934, vol. 23, pp. 637–64.
12. G. Wassermann: Über den Mechanismus der $\alpha \rightarrow \gamma$ Umwandlung des Eisens (On the Mechanism of the $\alpha \rightarrow \gamma$ Transformation of Iron). Mitteilungen aus dem Kaiser Wilhelm Institut für Eisenforschung, 1935, vol. 17, pp. 149–55.
13. A.B. Greninger and A.R. Troiano: *Metall. Trans.*, 1949, vol. 185, pp. 590–98.
14. G. Miyamoto, N. Iwata, N. Takayama, and T. Furuhara: *Acta Mater.*, 2010, vol. 58, pp. 6393–6403.
15. E.J. Payton, A. Aghajani, F. Otto, G. Eggler, and V.A. Yardley: *Scripta Mater.*, 2012, vol. 66, pp. 1045–48.
16. M.S. Wechsler, D.S. Lieberman, and T.A. Read: *Trans. AIME*, 1953, vol. 197, pp. 1503–15.

17. J.S. Bowles and J.K. Mackenzie: *Acta. Metall.*, 1954, vol. 2, pp. 129–37.
18. J.K. Mackenzie and J.S. Bowles: *Acta. Metall.*, 1954, vol. 2, pp. 138–47.
19. J.S. Bowles and J.K. Mackenzie: *Acta. Metall.*, 1954, vol. 2, pp. 224–34.
20. J.K. Mackenzie and J.S. Bowles: *Acta. Metall.*, 1957, vol. 5, pp. 137–49.
21. J.S. Bowles and J.K. Mackenzie: *Acta Metall.*, 1962, vol. 10, pp. 625–636.
22. Z. Nishiyama, M.E. Fine, and C.M. Wayman: *Martensitic Transformation*, Materials Science and Technology, Academic Press, Cambridge, 1978.
23. C.M. Wayman: *Introduction to the Crystallography of Martensitic Transformations*, Macmillan Series in Materials Science, Macmillan, London, 1964.
24. H. Kitahara, R. Ueji, M. Ueda, N. Tsuji, and Y. Minamino: *Mater. Charact.*, 2005, vol. 54, pp. 378–386.
25. M. Nikravesh, M. Naderi, and G.H. Akbari: *Mater. Sci. Eng.*, 2012, vol. 540, pp. 24–29.
26. L. Malet, M.R. Barnett, P.J. Jacques, and S. Godeta: *Scripta Mater.*, 2009, vol. 61, pp. 520–23.
27. G. Miyamoto, N. Takayama, and T. Furuhara: *Scripta Mater.*, 2009, vol. 60, pp. 1113–16.
28. A.H. Pham, T. Ohba, S. Morito, and T. Hayashi: *Mater. Char.*, 2017, vol. 132, pp. 108–18.
29. V.A. Yardley and E.J. Payton: *Mater. Sci. Technol.*, 2014, vol. 30, pp. 1125–30.
30. E. Gomes and L.A.I. Kerstens: *IOP Conf. Series: Mater. Sci. Eng.*, 2015, vol. 82, pp. 1–4.
31. N.Y. Zolotorevsky, S.N. Panpurin, A.A. Zisman, and S.N. Petrov: *Mater. Char.*, 2015, vol. 107, pp. 278–82.
32. T. Nyssönen, M. Isakov, P. Peura, and V.T. Kuokkala: *Met. Mater. Trans. A*, 2016, vol. 47, pp. 2587–90.
33. F. Bachmann, R. Hielscher, and H. Schaeben: *J. Appl. Crystallogr.*, 2010, vol. 43, pp. 1338–55.
34. E.C. Bain: *Trans. Am. Inst. Min. Met. Eng.*, 1924, vol. 70, p. 25.
35. T. Bayes: *Philos. Trans. R. Soc. Lond.*, 1764, vol. 53, pp. 370–428.
36. A.F. de Vos: Preprint, 2004.
37. B.M. Hill: *J. Am. Stat. Assoc.*, 1968, vol. 63, pp. 677–91.
38. B.A. Olshausen: Retrieved from: http://www.rctn.org/bruno/npb_163/bayes.pdf, 2004.
39. J.M. Bernardo and A.F.M Smith: Wiley, 2009.
40. N. Metropolis, A.W. Rosenbluth, M.N. Rosenbluth, A.H. Teller, and E. Teller: *J. Chem. Phys.*, 1953, vol. 21, pp. 1087–92.
41. W.K. Hastings: *Biometrika*, 1970, vol. 57, pp. 97–109.
42. C.J. Geyer: *Stat. Sci.*, 1992, vol. 7, pp. 473–511.
43. D. Gamerman and H. Lopes: Chapman and Hall/CRC, 2006.
44. A.F. Brust, S.R. Niezgoda, V.A. Yardley, and E.J. Payton: *Met. Trans. Mater. A*, 2018, vol. 50, pp. 837–55.
45. M. Natori, Y. Futamura, T. Tsuchiyama, and S. Takaki: *Scripta Mater.*, 2005, vol. 53, pp. 603–08.
46. A.F. Brust, T.J. Hobbs, E.J. Payton, and S.R. Niezgoda: *Microsc. Microanal.*, 2019, vol. 25, pp. 924–41.
47. R. Abrahams: Unit. Sts. Pat. Appl. Pub., US 2016/0369362 A1.
48. V. Sinha, E.J. Payton, M. Gonzales, R.A. Abrahams, and B.S. Song: *Metallogr. Microstruct. Anal.*, 2017, vol. 6 (6), pp. 610–18.
49. Y. He, Q. Rao, and Y. Tan: *J. Cent. South Univ. Technol.*, 1996, vol. 3, pp. 122–34.
50. G. Krauss: ASM International, 1990.
51. S. Matsuda, T. Inoue, H. Mimura and Y. Okamura: Climax Molybdenum Development Company, Ltd., Japan, 1971, pp. 45–66.
52. Z. Guo, CS. Lee, and JW. Morris: *Acta. Mater.*, 2004, vol. 52 (19), pp. 5511–18.
53. S. Morito, H. Yoshida, T. Maki, and X. Huang: *J. Mat. Sci. Eng. A*, 2006, vols. 438–440, pp. 237–40.
54. M. Ueda, H. Yasuda, and Y. Umakoshi: *Sci. Technol. Adv. Mater.*, 2001, vol. 3, pp. 171–79.

Publisher's Note Springer Nature remains neutral with regard to jurisdictional claims in published maps and institutional affiliations.